K. Regina[1]
Laboratory for Energy Conversion,
Department of Mechanical
and Process Engineering,
ETH Zurich,
Sonneggstrasse 3,
Zurich CH-8092, Switzerland
e-mail: regina@lec.mavt.ethz.ch

A. I. Kalfas
Department of Mechanical Engineering,
Aristotle University of Thessaloniki,
Thessaloniki GR-54124, Greece
e-mail: akalfas@auth.gr

R. S. Abhari
Laboratory for Energy Conversion,
Department of Mechanical
and Process Engineering,
ETH Zurich,
Sonneggstrasse 3,
Zurich CH-8092, Switzerland
e-mail: abhari@lec.mavt.ethz.ch

Experimental Investigation of Purge Flow Effects on a High Pressure Turbine Stage

In the present paper, an experimental investigation of the effects of rim seal purge flow on the performance of a highly loaded axial turbine stage is presented. The test configuration consists of a one-and-a-half stage, unshrouded, turbine, with a blading representative of high pressure (HP) gas turbines. Efficiency measurements for various purge flow injection levels have been carried out with pneumatic probes at the exit of the rotor and show a reduction of isentropic total-to-total efficiency of 0.8% per percent of injected mass flow. For three purge flow conditions, the unsteady aerodynamic flow field at rotor inlet and rotor exit has been measured with the in-house developed fast response aerodynamic probe (FRAP). The time-resolved data show the unsteady interaction of the purge flow with the secondary flows of the main flow and the impact on the radial displacement of the rotor hub passage vortex (HPV). Steady measurements at off-design conditions show the impact of the rotor incidence and of the stage flow factor on the resulting stage efficiency and the radial displacement of the rotor HPV. A comparison of the effect of purge flow and of the off-design conditions on the rotor incidence and stage flow factor shows that the detrimental effect of the purge flow on the stage efficiency caused by the radial displacement of the rotor HPV is dominated by the increase of stage flow factor in the hub region rather than by the increase of negative rotor incidence.
[DOI: 10.1115/1.4028432]

Introduction

In modern gas turbines, purge flow is bypassed from the compressor and injected through the stator/rotor rim seal in order to prevent the ingestion of hot gases from the main flow into the disk cavities between the rotors and the stators. By suppressing the ingress of hot gases into these cavities, the risk of local overheating of the materials and fatigue failures is minimized, leading to an increase of life time and ensuring a safe operation of these machines. In the past decades, the effects of mass flow through the rim seal have been analyzed in several publications.

One first main category of studies presented in this topic deals with the analysis of ingestion mechanisms and the identification of criteria upon which the level of ingestion into a stator–rotor wheelspace can be determined. Kobayashi et al. [1] give a minimum cooling air flow rate required to prevent ingress based on experimental data and a temperature fluctuation criterion. Based on a pressure criterion for a wheelspace without main flow, Chew et al. [2] derive a minimum sealant mass flow required for preventing ingestion due to disk pumping. The same authors isolate the effect of the external flow on the minimum sealant mass flow and derive a minimum sealant mass flow depending on the seal geometry and the rotational Reynolds number, see Dadkhah et al [3]. In a further step, Bohn et al. [4] isolate the effect which rotating blades have on the seal effectiveness of the purge flow, highlighting a measured reduction in effectiveness of up to 20% due to the presence of rotating blades and thus an increase of circumferential nonuniformities in the pressure near the hub end wall. For a transonic turbine, Gentilhomme et al. [5] have measured the seal effectiveness and have presented a model of ingestion. However, the authors report a higher ingestion in the measurements than predicted by the model especially at higher injection rates (IRs). The variation in the seal effectiveness with the operating point of a turbine is attributed to the change in main flow pressure ratio and has also been the focus of a study by Bohn et al. [6]. Numerical simulations are also taken into consideration when modeling the flow structures in wheelspaces: Jakoby et al [7] have presented numerical simulations and report the appearance of large scale unsteady features in the wheelspace if the sealant mass flow falls below a certain limit. Also, their numerical simulations led to an over prediction of experimentally measured seal effectiveness by 15–20%. The change in unsteadiness of the flow field of a turbine with HP/intermediate pressure (IP) steam turbine blading has also been the subject of investigations by Cao et al. [8]. The authors have concluded that the ingestion was suppressed and that the unsteadiness, which was resulting from flow structures of inside the cavity, was weakened when the axial clearance between the rotor and the stator was reduced.

A second main category of publications addresses the impact of the purge flow injection on the main flow of the turbine, highlighting the mixing mechanisms of the flows and quantifying the resulting performance of the turbine stages. Hunter and Manwaring [9] performed an experimental study on a two-stage low pressure (LP) turbine and reported the entrainment of low momentum cavity fluid into the HPVs of both rotors. The entrainment mechanism of the purge flow into HPVs was also reported in later studies on LP turbines, such as Schrewe et al. [10] for the case of the stator HPV and Jenny et al. [11] for the case of the rotor HPV. Several investigations of purge flow interaction mechanisms on HP turbine stages have also reported similar unsteady entrainment mechanisms and radial displacement of the rotor HPV. McLean et al. [12] have analyzed different types of injection configurations on a single stage HP turbine. When increasing the mass flow ratio of purge flow they found the changes in efficiency to be strongly dependent on the type of injection. For a variation of purge flow of up to 1% on a transonic single HP stage, Paniagua et al. [13] have attributed the increased lift off of the rotor HPV to the lower temperature of the purge flow as compared to the main flow. The low temperature has been made responsible for the transport of fluid to the suction side of the blade as well as for the strengthening of the intensity of the HPV and the enhanced

[1]Corresponding author.

Contributed by the International Gas Turbine Institute (IGTI) of ASME for publication in the JOURNAL OF TURBOMACHINERY. Manuscript received August 6, 2014; final manuscript received August 14, 2014; published online October 28, 2014. Editor: Ronald Bunker.

migration toward the middle of the channel. Reid et al. [14] have analyzed the purge flow effects on a single stage turbine with variable circumferential injection angle and identified two sources of loss mechanisms: the losses due to the mixing of the purge flow with the main flow and the losses due to the increased secondary flow through the rotor have been found to be equal. However, the authors warn when it comes to generalizing the findings to other turbines. Ong et al. [15] have attributed the strengthening of the rotor HPV and the increased penetration depth to the negative incidence caused by the purge flow. On different HP turbine stages, Ong et al. [15] and Schuepbach et al. [16] have shown the periodic nature of the increased displacement of the rotor HPV away from the end wall happening with vane passing frequency. In a 1.5-sage HP turbine, Schuepbach et al. [16] have demonstrated experimentally a decrease of efficiency by 0.6% per percent of injected mass flow based on measurements at two different purge flow IRs. The sensitivity of the stage efficiency with respect to the purge flow has been found to be even higher, −1.2% per percent of purge flow, when end wall contouring was used for the same turbine configuration as reported in Schuepbach et al. [17].

The current work experimentally quantifies the sensitivity of the isentropic total-to-total efficiency of a 1.5-satge HP turbine to the mass fraction of purge flow injected from the rotor upstream rim seal. In order to better understand the mechanisms of purge flow injection in a HP turbine stage, differences and similarities to the previous reports in literature regarding the steady and unsteady flow field analysis are highlighted.

Experimental Method

The experimental investigation was performed in the research axial turbine facility "LISA" in the Laboratory for Energy Conversion (LEC) at ETH Zurich. The one-and-a-half stage unshrouded turbine is representative for a high work, cooled turbine.

Research Turbine Facility. The research turbine facility consists of a quasi-closed air loop which includes a single stage radial compressor, a two-stage water-to-air heat exchanger and a calibrated venturi nozzle for accurate mass flow measurements. Upstream of the turbine test section, there is a 3-m-long flow conditioning stretch in order to ensure a homogenous flow field. In addition, the flow undergoes an acceleration ahead of the turbine to reduce the significance of any remaining flow nonuniformities from upstream. At the exit of the turbine test section, the air loop is open to atmospheric conditions. A DC generator absorbs the turbine's power and controls the rotational speed with an indicated accuracy of ±0.02% (±0.5 rpm). The water-to-air heat exchanger controls the inlet total temperature $T_{0,in}$ to an accuracy of ±0.3 K. A torquemeter measures the torque on the rotor shaft. Since the compressor ratio is limited to $\Pi_{c,max} = 1.5$, it is necessary to add a tandem deswirl vane arrangement to recover the static pressure at the exit of the second nozzle guide vane (NGV) back to the ambient level in order to reach the intended pressure ratio of $\Pi_{1.5} = 1.65$. The unshrouded rotor has a nominal tip gap of 1% of the span and the variation of the tip gap between different assemblies is less than 1% of the tip gap ensuring good repeatability. At the exit of the first NGV, the flow is compressible with an averaged exit Mach number of 0.53.

The current turbine configuration is derived from the turbine design presented by Behr et al. [18]. The most salient differences are an increased blade row spacing between the NGV 1 and the rotor as well as an increased axial clearance at the exit of the hub cavity, where the purge flow is injected. In Fig. 1, the tested geometry of the rotor can be seen.

Operating Conditions. During the measurements, the turbine 1.5-stage total-to-static pressure ratio is kept constant at $\Pi_{1.5} = 1.65$ in order to account for the change in ambient pressure on different days. With the same purpose, the pressures are nondimensionalized by the respective inlet stagnation pressure. The main operating parameters are summarized in Table 1.

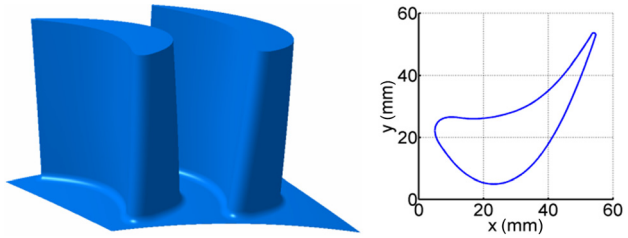

Fig. 1 Tested rotor geometry isometric view (left) and profile at 6% span (right)

The purge flow injected from the upstream stator/rotor cavity is an off-take from the primary air loop upstream of the flow conditioning stretch and is measured by means of a standard nozzle. The bypassed air passes a plenum and is fed through ten different NGVs into the cavity underneath the NGV platform, labeled as B in Fig. 2, where a schematic of the purge flow path is depicted.

After the purge flow enters the under platform cavity, there are two paths, which are indicated by dotted arrows in Fig. 2. One path is through the upstream rim seal into the main flow, labeled as P. The rest of the gas, called secondary mass flow and labeled as S in Fig. 2, is ejected through the drum to the atmosphere, after being measured in an additional standard nozzle. Since the pressure difference across the downstream rim seal is controlled to be zero, the net mass flow through the downstream rim seal can be assumed to be zero. As a consequence, the mass flow P eventually injected into the main flow can be calculated as the difference between the measured bypass mass flow B and the measured secondary mass flow S.

In the present investigation, the injection levels were defined by means of the IR defined by the following equation:

$$IR = \frac{\dot{m}_B - \dot{m}_S}{\dot{m}_{\mathrm{MAIN}}} \times 100 \tag{1}$$

The current tests have been conducted with IR1 = −0.1% representing a moderate sucking from the main flow, as well as with IR2 = 0.8% and IR3 = 1.2%, which are considered to be representative for real engine conditions.

Measurement Technology. The steady flow field at the exit of the rotor is measured with a miniature cobra-head five-hole probe (5 HP) with a tip diameter as small as 0.9 mm, whereas at the inlet of the rotor a pneumatic miniature four-hole probe (4 HP) with a cylindrical head and a diameter of 1.8 mm is used.

The unsteady flow field measurements are performed using a FRAP, which was developed in-house at the LEC at ETH Zurich. Details on the FRAP and measurement technique are presented in depth in Refs. [19] and [20]. The FRAP is capable of capturing the unsteady flow features up to frequencies of 48 kHz based on measurements including the total and static pressures, flow yaw

Table 1 Operating conditions and geometrical characteristics

Pressure ratio $\Pi_{1.5}$	1.65 ± 0.4%	—
Inlet total temperature $T_{0,in}$	327.9 ± 0.3	(K)
Capacity $\frac{\dot{m}\sqrt{T_{0,in}}}{p_{0,in}}$	151.8 ± 0.2	$\left(\frac{kg \cdot K^{1/2}}{s \cdot bar}\right)$
Nondimensional speed $\frac{N}{\sqrt{T_{0,in}}}$	2.49 ± 0.05	$\left(\frac{rps}{K^{1/2}}\right)$
Mach nr (S1 ex/R ex/S2 ex)	0.53/0.26/0.48	
Reynolds number (S1/R/S2)	7.1/3.8/5.1	($\times 10^5$)
Blade count (S1/R/S2)	36/54/36	—
Aspect ratio (S1/R/S2)	0.87/1.17/0.82	—

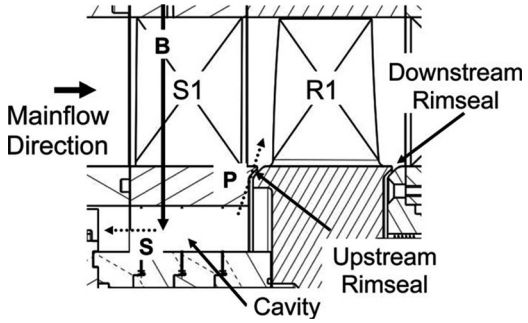

Fig. 2 Schematics of the purge flow path [16] (not to scale)

and pitch angles, and Mach number. The frequency bandwidth of the temperature is limited to a frequency of 10 Hz. However, the influence of the measured temperature on the velocity is judged to be very modest. The FRAP has a 1.8 mm tip diameter and is equipped with two miniature silicon piezoresistive sensors. The probe is operated in a virtual-4-sensor mode to measure the three-dimensional, time-resolved flow properties. The data is acquired at a sampling rate of 200 kHz over a period of time of 2 s. The postprocessing is done for three consecutive rotor pitches. The sampling rate resolves 82 points in the rotor relative frame of reference (FOR). The typical measurement uncertainties obtained with the FRAP for a calibration range of ±24 deg for the yaw angle and ±20 deg for the pitch angle are given in Table 2. The relative uncertainties of the total and static pressures are given as a percentage of the dynamic head.

The measurement data are acquired at two different axial locations in the turbine test facility by traversing the probe in radial and circumferential direction. The first traverse plane, labeled with "R in," is located downstream of the first NGV at a distance of 32% of the axial chord of the NGV. This axial location coincides with the platform leading edge of the rotor. The second traverse plane, labeled with "R ex," is located downstream of the rotor at a distance of 16% of the rotor axial chord. The spatial resolution of the measurement grid at the traverse planes consisted of 38 radial and 41 circumferential points covering one NGV 1 pitch. The circumferentially points are equally spaced whereas the radial points are clustered near the end walls.

Results and Discussions

In the frame of the current study, also the unsteady flow field at the inlet of the rotor shall be analyzed and discussed in order to better understand how the complex mechanisms of purge flow are initiated and eventually cause the well reported effects on the rotor HPV.

As mentioned by Cao et al. [8] and shown by Schuepbach et al. [16], the purge flow mixing process has a clear impact on the unsteadiness of the flow field. Therefore, the rms values of the random part of the pressure signal acquired by the FRAP have shown to be an appropriate indicator for the purge flow injection mechanisms. Based on the triple decomposition of the time-resolved pressure signal $p(t)$ as shown in Eq. (2), the random part of the signal $p'(t)$ can be calculated as the difference between the time-resolved signal $p(t)$ and the phase-locked averaged pressure signal $\bar{p}(t) + \tilde{p}(t)$. More details on this approach can be found in Porreca et al. [21], where it is used to derive turbulent quantities

Table 2 Relative uncertainty bandwidth of the FRAP

Yaw angle	Pitch angle	P_t	P_s
0.24 deg	0.36 deg	1%	1.2%

$$p(t) = \bar{p}(t) + \tilde{p}(t) + p'(t) \tag{2}$$

In the following, the rms of the random part of the pressure signal of the central hole (p'_1) will be used.

Rotor Inlet. The time-averaged rms of p'_1 at the inlet of the rotor is depicted in Fig. 3 for the IR1 and IR3 case.

A comparison of both purge flow cases reveals clear differences in the unsteadiness of the flow field already at the inlet of the rotor. Since this measurement plane is located above the platform leading edge of the rotor, the initiated mixing process of the purge flow with the main flow has already started and is captured. Therefore, differences in the flow field can be attributed to the purge flow. It is remarkable that the purge flow has increased the unsteadiness across the complete circumference.

When looking at the circumferentially mass averaged distribution of the above depicted quantity, the radial extent of impact of the purge flow becomes more evident, as shown in Fig. 4.

The radial distribution shows the increase of unsteadiness reaching spanwise positions of up to midspan and showing an increase in the peak of up to 100% at lower span positions. The increase of unsteadiness with the increase of injected purge mass flow shows an opposite trend as described by Cao et al. [8] for the case of hub pressure unsteadiness in a turbine stage with ingestion. The authors of Ref. [8] concluded that if ingestion was happening, causing a strong unsteady flow structure inside the wheelspace, then the unsteadiness of the pressure at the hub should decrease if the sealant flow is increased, since the ingestion would be more and more suppressed.

When comparing ingestion-relevant parameters of the current test cases to minimum required values documented in the literature, ingestion should not be expected to play a significant role in the conducted experimental investigations.

According to the pressure criterion used by Dadkhah et al. [3], the present nondimensionalized injected mass flow of $C_w = 14000$ (IR2) is 60% above the minimum sealing flow required for the high external flow Reynolds number of $Re_w = 3.8 \times 10^6$ and for the given seal geometry of the test case. This safety margin also can take into account the reduction in seal effectiveness of about 20% due to the influence of the rotating blades as reported by Bohn et al. [4]. Also, the present volumetric flow rate of about

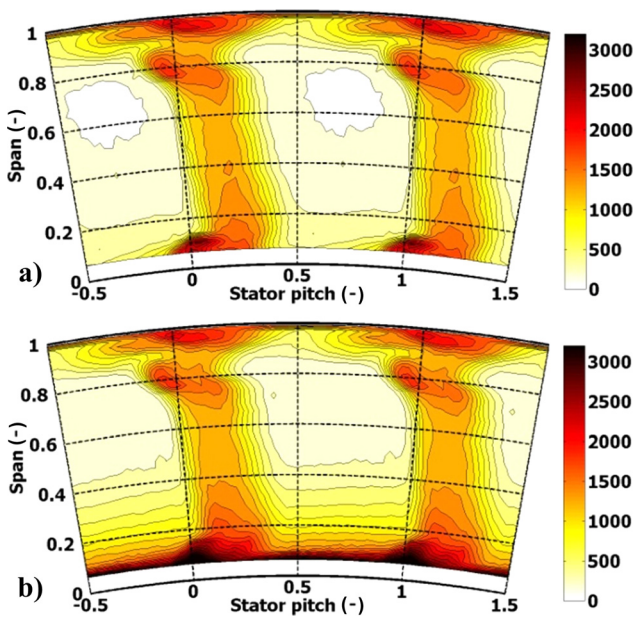

Fig. 3 Time-averaged rms of p_1' (Pa) in stationary FOR at plane R in (*a*) IR1 = −0.1% and (*b*) IR3 = 1.2%

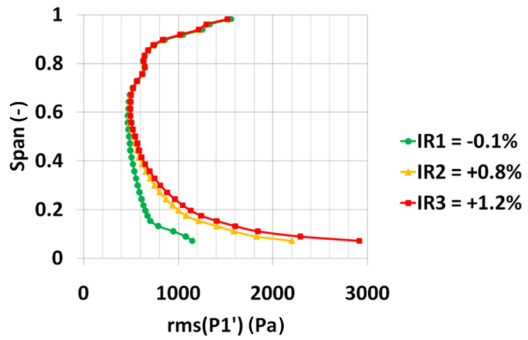

Fig. 4 Time-averaged and circumferentially mass averaged rms of p_1' (Pa) at plane *R* in

80 m^3/s (IR2) is above the minimum cooling air flow as reported by Kobayashi et al. [1] for a rotational Reynolds number $Re_\Phi = 1.8 \times 10^6$. Based on these observations, it seems legitimate to assume that no significant ingestion is present in the current test cases and that the unsteadiness at the rotor inlet is in fact resulting from the unsteady injection mechanism of the purge flow into the main flow and the mixing phenomena related thereto.

In order to further analyze the interaction of the purge flow with the periodic fluctuations coming from the rotor, the time-resolved data at the rotor inlet shall be discussed. At a spanwise position of 6% span, which is the lowest spanwise position accessible by the probes, it can be seen that the flow field is dominated by the secondary flow features of the upstream NGV, since the traces of high rms of p_1' visible in Fig. 5 are vertical.

At about 0 pitch (and 1 pitch) the traces of the NGV HPV can be seen and the time evolution shows the periodic modulation by the rotor, since for a constant circumferential position the rms of p_1' is fluctuating with rotor blade passing period. Also the region of the wake is visible as fluid with a slightly increased rms of p_1' ranging until about 0.3–0.4 pitch.

However, when injecting purge flow at the IR3 = 1.2% the region of the flow field unaffected by the secondary flow features of the NGV 1 also becomes modulations by the rotor as can be seen in Fig. 5 by the inclined traces of high rms of p_1'. These regions of high rms of p_1' are a result of the purge flow and the fact that the mixing process of the purge flow with the main flow is happening with rotor blade passing frequency since the pressure gradient pushing the main flow through the cavity is determined by the periodic rotor potential field.

An impact of the purge flow on the downstream blade row, which is commonly discussed in literature, is the change in incidence of the fluid, since the purge flow enters the main flow without any preconditioning and as a low momentum fluid, leading to a reduced relative flow yaw angle when the fluid near the end walls reaches the rotor blade. For the current test conditions analyzed, the introduction of purge flow caused a change in incidence of up to approx. $\Delta i = -3$ deg at the lower spanwise positions, as can be seen in the time-averaged and circumferentially mass averaged relative flow yaw angle in Fig. 6.

In order to allow a further evaluation of the impact of the change in incidence on the downstream blade row a discussion of the time-resolved evolution of the relative flow yaw angle is appropriate. Again for the lowest accessible spanwise position, in Fig. 7, the time-resolved relative flow yaw angle for the IR1 and IR3 purge flow conditions are shown.

The comparison of the relative flow yaw angle for the two IRs shows that the periodic interaction mechanisms of the purge flow do not change substantially the qualitative time-resolved behavior of the relative flow yaw angle. Despite the changes observed in the rms of p_1', the secondary flow structures of the NGV appear with the same underturning effect. However, it can be seen that the purge flow reduces the peak-to-peak variation of the relative flow yaw angle.

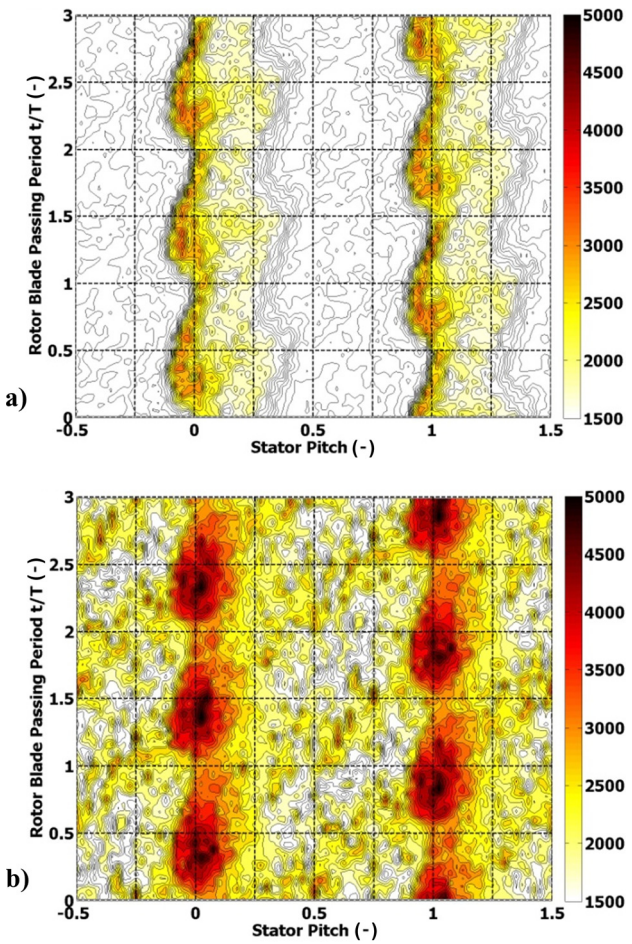

Fig. 5 Time-resolved rms of p_1' (Pa) at 6% span in stationary FOR at plane R in (*a*) IR1 = −0.1% and (*b*) IR3 = 1.2%

Rotor Exit. In this section, the most relevant observations of the flow field at the exit of the rotor will be discussed in order to conclude on the source of the isentropic total-to-total efficiency deficit caused by the purge flow.

In Fig. 8, the contour diagrams of the normalized relative total pressure are shown for the IR1 and IR3 conditions.

In the contour diagrams of Fig. 8, the traces of the tip leakage vortex and the tip passage vortex are seen at approximately 95% span and 70% span, respectively. However, the secondary flow

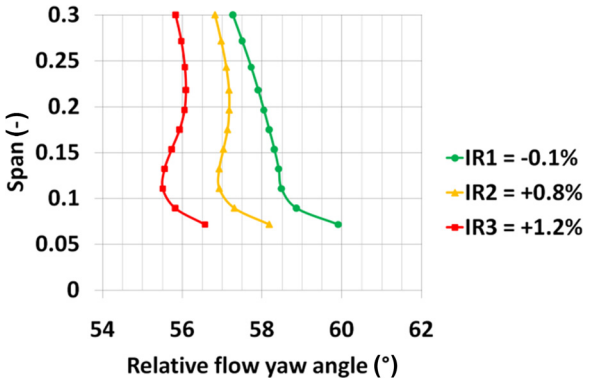

Fig. 6 Time-averaged and circumferentially mass averaged relative flow yaw angle (deg) at plane R in

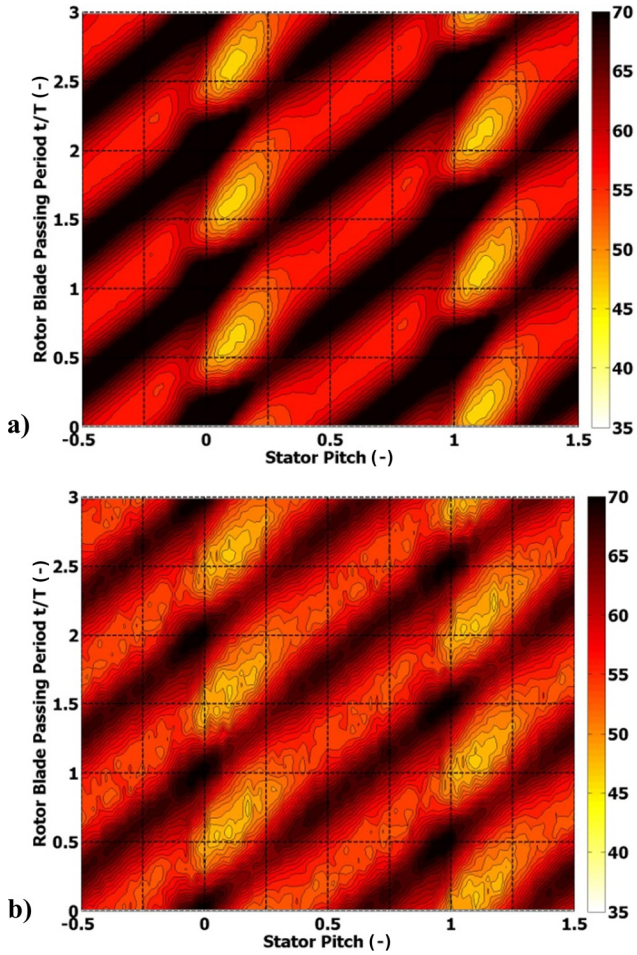

Fig. 7 Time-resolved relative flow yaw angle (deg) at 6% span in stationary FOR at plane R in (*a*) IR1 = −0.1% and (*b*) IR3 = 1.2%

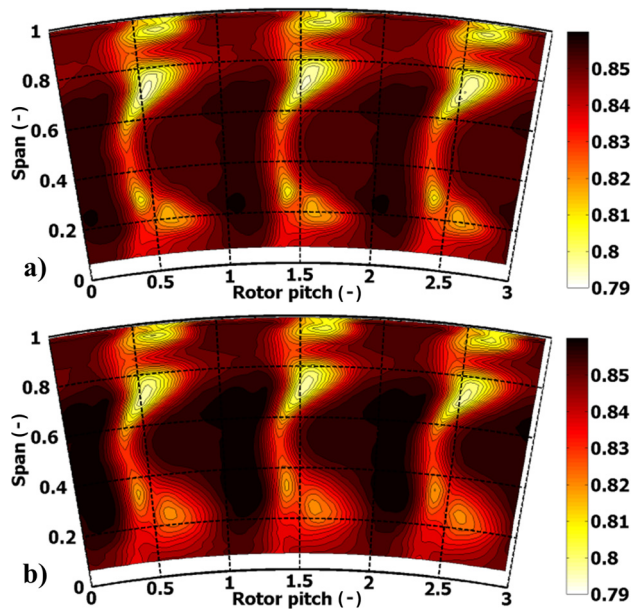

Fig. 8 Time-averaged normalized relative total pressure in rotating FOR at plane R ex (*a*) IR1 = −0.1% and (*b*) IR3 = 1.2%

features influenced the most by the injected purge flow are the wake and the rotor HPV at about 20% span. The increase in size of the rotor HPV and its radial displacement toward midspan, which are caused by the injection of the purge flow, confirm the previous findings well documented in the literature. The change in radial lift-off of the rotor HPV induced by the purge flow injection resulted to about 4% span.

When analyzing the time-resolved data, the periodic interaction with the purge flow and the secondary flow features of the rotor becomes more and more visible the higher the IR. For demonstrating this effect, the time-resolved rms of p_1' is depicted in Fig. 9 for radial traverses at two different circumferential locations in the stationary FOR. The first location is characterized by showing little interaction of the secondary flow features of the rotor and stator whereas in the second one it is high.

The comparison of the time-resolved evolution of the secondary flows shows a higher level of unsteadiness in the secondary flow features of the rotor for the second location across the entire span. For this circumferential location, the secondary flow features of the upstream NGV are present confirming the fact that the low momentum fluid of the NGV 1 is caught up in the secondary flow features of the rotor. Furthermore, the location of the core of the rotor HPV at about 20% span shows a radial displacement of approximately 7% span when comparing both circumferential locations. Since this periodical radial lift-off of the rotor HPV with vane passing frequency starts to appear with higher IRs, it can be attributed to the purge flow rather than to the secondary flow features of the vane. This is in very good agreement

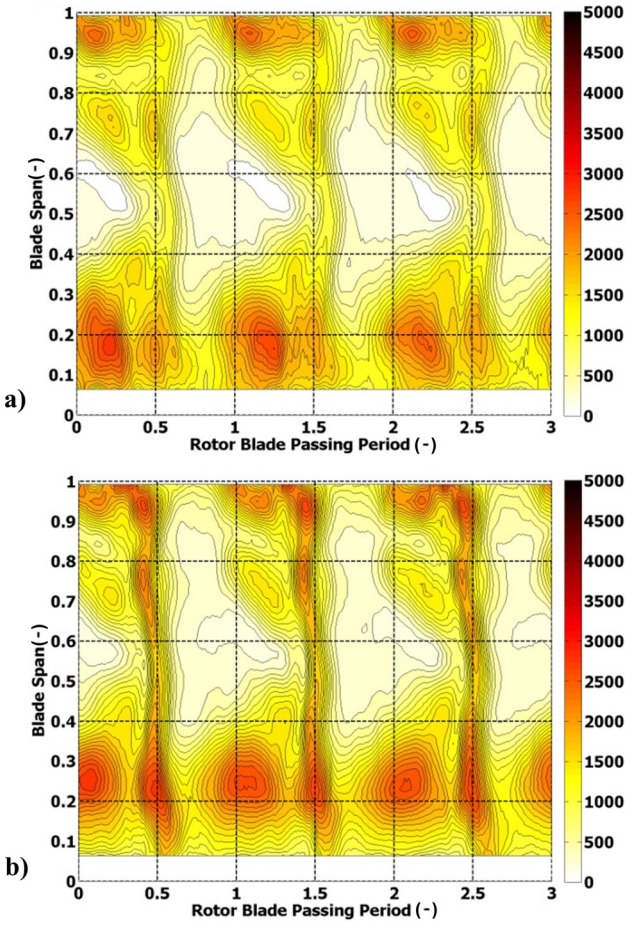

Fig. 9 Time-resolved rms of p_1' (Pa) in stationary FOR at plane R ex for IR3, locations where the interaction with the NGV 1 secondary flow features is (a) low and (b) high

to the reports by Ong et al. [15], Schuepbach et al. [16], and Jenny et al. [11].

The detrimental impact of the purge flow injection on the performance of the rotor shall be quantified by means of the isentropic total-to-total stage efficiency as defined by Eq. (3), in which the enthalpy drop of the purge flow is also taken into account

$$\eta_{tt} = \frac{\omega \cdot M}{\dot{m}_{\mathrm{MAIN}} \cdot c_{\mathrm{p}} \cdot T_{0,\mathrm{in}}} \Bigg/ 1 - \left(1 - \frac{IR}{100}\right) \cdot \left(\frac{p_{0,R_{\mathrm{ex}}}}{p_{0,\mathrm{in}}}\right)^{(\gamma-1)/\gamma} - \frac{IR}{100} \cdot \left(\frac{p_{0,R_{\mathrm{ex}}}}{p_{0,\mathrm{cav}}}\right)^{(\gamma-1)/\gamma} \quad (3)$$

For studying the sensitivity of the stage performance toward the percentage of injected mass flow, more IRs were tested than those for the detailed and time-resolved measurements discussed above. The time-averaged and circumferentially mass averaged measurements of the total-to-total efficiency by means of a high accuracy five-hole probe are shown in Fig. 10.

The gradual strengthening of the rotor HPV with the increase of purge flow IR is clearly visible by the gradual drop in efficiency at the lower spanwise positions. Also, the continuous increase in lift-off of the rotor HPV is captured and can be seen by an increase of the radial location of minimal efficiency by approximately 4% span when comparing the case with moderate sucking to the case of IR = 1.2%, which shows an excellent agreement with the above described measurements with the time-resolved probes.

However, the sensitivity of the penetration depth of the rotor HPV in the current test cases, which can be indicated with 3% span per percent of injected purge flow, is somewhat lower than the value of about 7% from the experimental results by Ong et al. [15] for a single stage HP turbine. Also higher is the sensitivity of 7–10% per percent of injected purge flow indicated by Jenny et al. [11] for a stage with blading representative for a LP turbine but with similar operating conditions as the turbine for the current investigations.

The overall sensitivity of the stage efficiency to the purge flow is depicted in Fig. 11.

The measured values confirm the commonly identified linear trend of the efficiency drop with increasing injection ratio. The overall sensitivity calculated based on a linear regression is $\Delta\eta_{\mathrm{tt}} = -0.8\%$ per percent of injected purge flow. For a turbine stage with the same airfoils but with a lower axial blade row spacing between the NGV 1 and the rotor and with a reduced axial clearance of the rim seal, Schuepbach et al. [16] have measured a lower sensitivity of $\Delta\eta_{\mathrm{tt}} = -0.6\%$ per percent of injected purge flow. This change in sensitivity has not been studied yet, but is currently being associated with the different axial rim seal clearance.

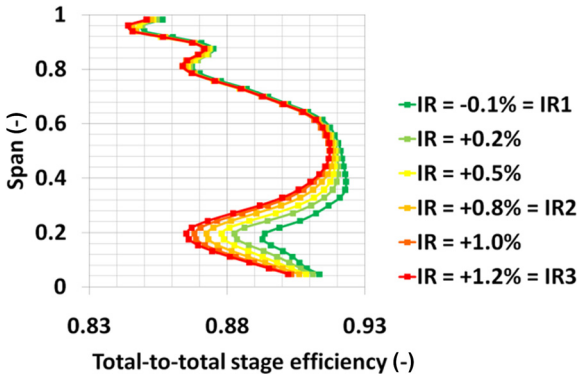

Fig. 10 Time-averaged and circumferentially mass averaged isentropic total-to-total stage efficiency at plane R ex

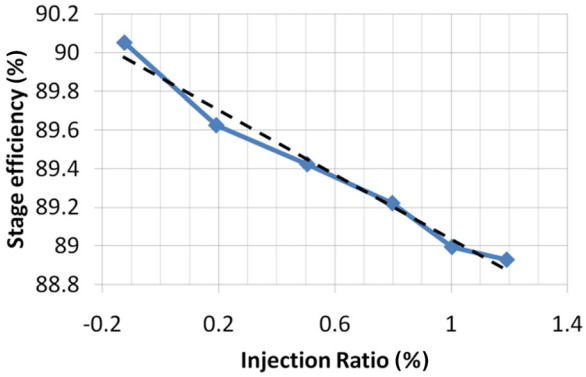

Fig. 11 Sensitivity of the isentropic total-to-total stage efficiency toward the IR

Incidence Sensitivity of the Rotor. It is well documented in literature that different parameters play an important role in the interaction mechanisms involved when purge flow is injected through the rim seal into the main flow of a turbine stage. Most commonly mentioned are the one-dimensional parameters such as the ratio of the purge mass flow and the main flow, the nondimensional mass flow rate C_{w}, or the rotational Reynolds number. However, when it comes to the explanation of the sources of the periodic impact of the purge flow on the development and migration of the rotor HPV, the change of the flow field incoming to the rotor is often mentioned, especially due to the change in incidence caused by the low momentum fluid injected.

For the purpose of highlighting the effect of the incidence on the performance of the current HP turbine, a further analysis of two off-design tests shall be considered and compared to the off-design effect caused by the purge flow near the hub end wall. In the nominal point (IR2), the spanwise averaged degree of reaction is 35%, whereas the local degree of reaction at the lowest accessible spanwise position amounts to 30%. The two additional operating points cause a reduction/increase of incidence on the rotor by approximately ±6 deg as well as an increase/reduction of degree of reaction by approximately +3%/−14%. The conditions are summarized in Table 3.

At lower spanwise position, a result with similar trends as when varying the purge flow can be observed, especially when looking at the impact on stage efficiency. Therefore, the time-averaged and circumferentially mass averaged isentropic total-to-total stage efficiency is shown in Fig. 12.

For the variation of incidence tested, it is clear that the same trends as discussed before are observed. The change in operating point of the rotor causes in a combined manner:

(1) a strengthening of the rotor HPV, seen by a lower stage efficiency in the loss core together with
(2) an increase of the radial displacement of the loss core toward midspan.

However, when associating these trends at the exit of the rotor to the changes in the flow field at the inlet of the rotor, it becomes obvious that the trends caused by purge flow variation and caused

Table 3 Nominal and off-design operating points

	$\Delta i = 0$	$\Delta i < 0$	$\Delta i > 0$
Speed (rpm)	2700	2700	1900
Mass flow (kg/s)	11.6	9.6	9.6
Injection rate IR (%)	0.8	0.8	0.8
Flow coefficient Φ	0.56	0.48	0.71
Loading coefficient Ψ	2.34	1.85	3.14

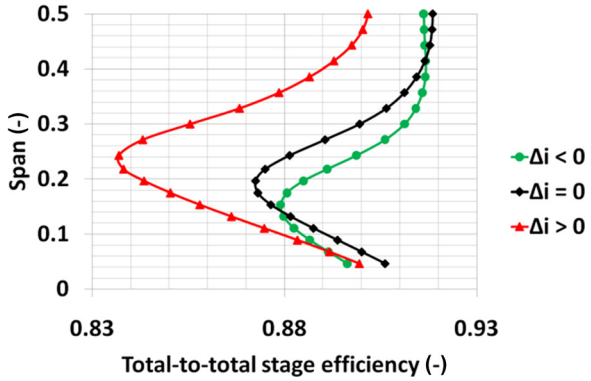

Fig. 12 Time-averaged and circumferentially mass averaged isentropic total-to-total stage efficiency at plane R ex

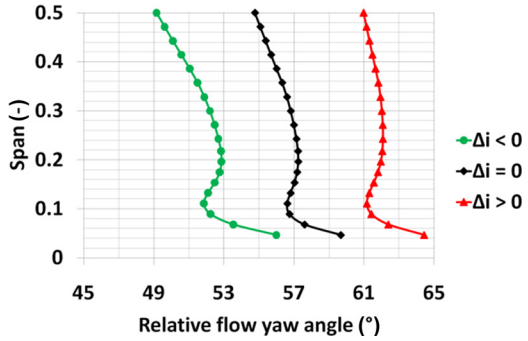

Fig. 13 Time-averaged and circumferentially mass averaged relative flow yaw angle (deg) at plane R ex

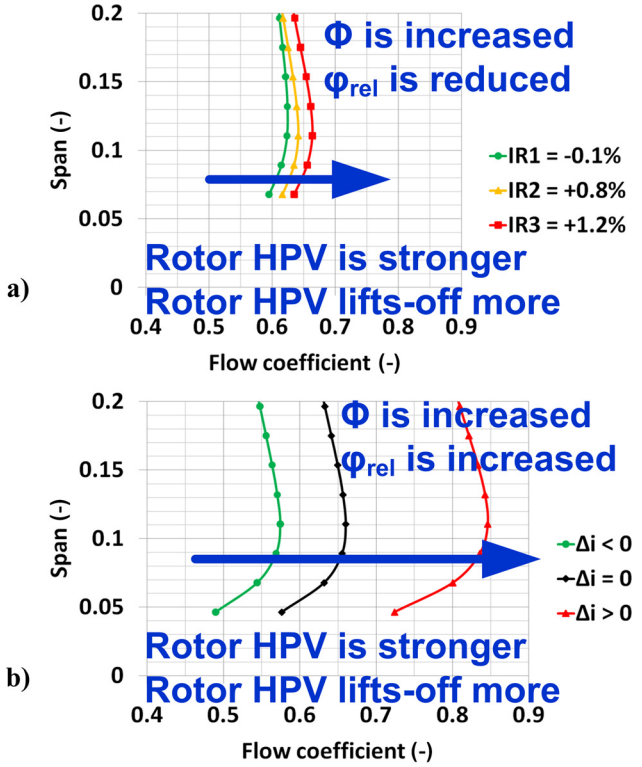

Fig. 14 Time-averaged and circumferentially mass averaged flow coefficient (*a*) due to variation of purge flow and (*b*) due to variation of overall operating point

by variation of operating point are opposed if the change in incidence is looked at. Therefore, Fig. 13 shows the time averaged and circumferentially mass averaged relative flow yaw angle at the inlet to the rotor.

In the region close to the hub, the off-design condition with a reduction of main mass flow causes a reduction of relative flow yaw angle by about $\Delta i = -4$ deg which is in the same range as the purge flow variation has caused ($\Delta i = -3$ deg). Therefore, if a strengthening of the rotor HPV and an increase of its penetration depth had to be explained with changes in incidence, for the current rotor and the operation point, a reduction of relative flow yaw angle should be beneficial for the evolution of the rotor HPV as shown by the off-design tests. The purge flow injection shows an opposite, detrimental effect though. As a consequence, the lift-off of the rotor HPV due to increasing the IR cannot be attributed to the change in incidence induced by the purge flow.

However, the same trends of evolution of the rotor HPV are observed when comparing the effect of the variation of purge flow and operating point if the flow coefficient of the stage is looked at, see Fig. 14, where the effects due to purge flow and due to the changes in the overall operating point are shown.

The trends observed in Fig. 14 suggest that the relevance of the stage flow coefficient is judged to be considerable when explaining the increase in penetration depth of the rotor HPV and its strengthening since both experimental variations reveal the same trends. If a two-dimensional design parameter had to be used for reproducing correctly the effect of the purge flow on the downstream blade row, then the flow coefficient, which can be interpreted as a nondimensionalized mass flow rate, is considered to be appropriate. Although the low momentum fluid injected from the hub does in fact cause a negative change in incidence, resulting in a benefit for the rotor under the operating conditions studied, it also increases the mass flow which is transported close to the end walls of the rotating passage. As a consequence, additional mass flow is caught up in the rotor HPV causing its strengthening and further penetration into the rotor passage as it convects through the blade passage.

Conclusions

The results presented in this paper are based on time-resolved measurements by means of FRAP conducted in a one-and-a-half stage research axial turbine. The tested configuration was equipped with blading representative for HP gas turbines and with injection of purge flow through the rotor upstream rim seal at IRs of -0.1% representing a moderate sucking as well as of $+0.8\%$ and $+1.2\%$ representing engine realistic conditions.

Based on high accuracy five-hole probe measurements, the detrimental effect of the purge flow injection has been quantified and amounts to $\Delta\eta_{tt} = -0.8\%$ per percent of injected purge flow. Based on the time-resolved measurements for an IR of 1.2%, a periodic variation with vane passing frequency of the penetration depth of the rotor HPV by 7% span has been captured. At this IR, the time-averaged increase in penetration depth sums up to 4%.

Tests of the rotor at overall off-design conditions have indicated the sensitivity direction of the stage efficiency when changing the incidence on the rotor and flow coefficient of the stage in a combined way. These tests have shown a beneficial impact of negative changes in incidence on the stage efficiency and evolution of the rotor HPV. Therefore, if a two-dimensional design parameter had to be identified for indicating the detrimental impact of the evolution of the rotor HPV on the isentropic stage efficiency caused by the injection of purge flow, then the flow factor rather than the incidence change seems to be appropriate.

Acknowledgment

The authors gratefully acknowledge the permission of Siemens and MTU to publish the data and especially the contributions and support from Matthew Montgomery and Carsten Zscherp.

Nomenclature

c_{ax} = axial flow velocity
c_p = specific heat capacity
$C_w = \dot{m}_{cool}/\mu R$ = nondimensional coolant flow
$\bar{c}_{abs}$ = mean absolute flow velocity
i = incidence angle
IR = injection rate
M = torque
$\dot{m}$ = mass flow
N = rotational speed
p = pressure
R = hub radius
$Re_w = \rho \bar{c}_{abs} R/\mu$ = external flow Reynolds number
$Re_\Phi = \rho \omega R^2/\mu$ = rotational Reynolds number
T = temperature
U = local rotational speed
γ = isentropic coefficient
η = isentropic efficiency
μ = dynamic viscosity
Π = pressure ratio
ρ = density
ϕ = flow yaw angle
$\Phi = c_{ax}/U$ = flow coefficient
$\psi = \Delta H/U^2$ = loading coefficient
ω = angular frequency

Subscripts

in = turbine inlet flow quantity
rel = relative frame flow quantity
tt = total-to-total
0 = stagnation flow quantity

Abbreviations

FOR = frame of reference
FRAP = fast response aerodynamic probe
HP = high pressure
HPV = hub passage vortex
IP = intermediate pressure
LP = low pressure
NGV = nozzle guide vane

References

[1] Kobayashi, N., Matsumato, M., and Shizuya, M., 1984, "An Experimental Investigation of a Gas Turbine Disk Cooling System," ASME J. Eng. Gas Turbines Power, **106**(1), pp. 136–141.
[2] Chew, J. W., Dadkhah, S., and Turner, A. B., 1992, "Rim Sealing of Rotor–Stator Wheelspaces in the Absence of External Flow," ASME J. Turbomach., **114**(2), pp. 433–438.
[3] Dadkhah, S., Turner, A. B., and Chew, J. W., 1992, "Performance of Radial Clearance Rim Seals in Upstream and Downstream Rotor–Stator Wheelspaces," ASME J. Turbomach., **114**(2), pp. 439–445.
[4] Bohn, D., Rudzinski, B., Sürken, N., and Gärtner, W., 2000, "Experimental and Numerical Investigation of the Influence of Rotor Blades on Hot Gas Ingestion Into the Upstream Cavity of an Axial Turbine Stage," ASME Paper No. 2000-GT-0284.
[5] Gentilhomme, O., Hills, N. J., Turner, A. B., and Chew, J. W., 2003, "Measurement and Analysis of Ingestion Through a Turbine Rim Seal," ASME J. Turbomach., **125**(3), pp. 505–512.
[6] Bohn, D. E., Decker, A., Ohlendorf, N., and Jakoby, R., 2006, "Influence of an Axial and Radial Rim Seal Geometry on Hot Gas Ingestion Into the Upstream Cavity of a 1.5-Stage Turbine," ASME Paper No. GT2006-90453.
[7] Jakoby, R., Zierer, T., Lindblad, K., Larsson, J., deVito, L., Bohn, D. E., Funcke, J., and Decker, A., 2004, "Numerical Simulation of the Unsteady Flow Field in an Axial Gas Turbine Rim Seal Configuration," ASME Paper No. GT2004-53829.
[8] Cao, C., Chew, J. W., Millington, P. R., and Hogg, S. I., 2003, "Interaction of Rim Seal and Annulus Flows in an Axial Flow Turbine," ASME Paper No. GT2003-38368.
[9] Hunter, S. D., and Manwaring, S. R., 2000, "Endwall Cavity Flow Effects on Gaspath Aerodynamics in an Axial Flow Turbine: Part I—Experimental and Numerical Investigation," ASME Paper No. 2000-GT-0651.
[10] Schrewe, S., Linker, C., Krichbaum, A., and Schiffer, H.-P., 2011, "Measurements of Rim Seal Mixing Processes in an Axial Two Stage Turbine," 20th International Symposiumm on Air Breathing Engines (ISABE 2011), Gothenburg, Sweden, Sept. 12–16, Paper No. ISABE-2011-1720.
[11] Jenny, P., Abhari, R. S., Rose, M. G., Brettschneider, M., Gier, J., and Engel, K., 2011, "Low-Pressure Turbine End Wall Design Optimisation and Experimental Verification in the Presence of Purge Flow," 20th International Symposiumm on Air Breathing Engines (ISABE 2011), Gothenburg, Sweden, Sept. 12–16, Paper No. ISABE-2011-1717.
[12] McLean, C., Camci, C., and Glezer, B., 2001, "Mainstream Aerodynamic Effects Due to Wheelspace Coolant Injection in a High-Pressure Turbine Stage: Part I—Aerodynamic Measurements in the Stationary Frame," ASME J. Turbomach., **123**(4), pp. 687–696.
[13] Paniagua, G., Dénos, R., and Almeida, S., 2004, "Effect of the Hub Endwall Cavity Flow on the Flow-Field of a Transonic High-Pressure Turbine," ASME J. Turbomach., **126**(4), pp. 578–586.
[14] Reid, K., Denton, J., Pullan, G., Curtis, E., and Longley, J., 2006, "The Effect of Stator–Rotor Hub Sealing Flow on the Mainstream Aerodynamics of a Turbine," ASME Paper No. GT2006-90838.
[15] Ong, J. H. P., Miller, R. J., and Uchida, S., 2006, "The Effect of Coolant Injection on the Endwall Flow of a High Pressure Turbine," ASME Paper No. GT2006-91060.
[16] Schuepbach, P., Abhari, R. S., Rose, M. G., Germain, T., Raab, I., and Gier, J., 2010, "Effects of Suction and Injection Purge-Flow on the Secondary Flow Structures of a High-Work Turbine," ASME J. Turbomach., **132**(2), p. 021021.
[17] Schuepbach, P., Abhari, R. S., Rose, M. G., and Gier, J., 2011, "Influence of Rim Seal Purge Flow on the Performance of an Endwall-Profiled Axial Turbine," ASME J. Turbomach., **133**(2), p. 021011.
[18] Behr, T., Kalfas, A. I., and Abhari, R. S., 2007, "Unsteady Flow Physics and Performance of a One-and-1/2-Stage Unshrouded High Work Turbine," ASME J. Turbomach., **129**(2), pp. 348–359.
[19] Kupferschmied, P., Köppel, P., Gizzi, W., Roduner, C., and Gyarmathy, G., 2000, "Time-Resolved Flow Measurements With Fast-Response Aerodynamic Probes in Turbomachines," Meas. Sci. Technol. **11**(7), pp. 1036–1054.
[20] Pfau, A., Schlienger, J., Kalfas, A. I., and Abhari, R. S., 2003, "Unsteady 3-Dimensional Flow Measurement Using a Miniature Virtual 4 Sensor Fast Response Aerodynamic Probe (FRAP)," ASME Paper No. GT2003-38128.
[21] Porreca, L., Hollenstein, M., Kalfas, A. I., and Abhari, R. S., 2007, "Turbulence Measurements and Analysis in a Multistage Axial Turbine," J. Propul. Power, **23**(1), pp. 227–234.